

Higher-Order Topological Mott Insulator on the Pyrochlore Lattice

Yuichi Otsuka,^{1,2,*} Tsuneya Yoshida,^{3,4} Koji Kudo,⁴ Seiji Yunoki,^{1,2,5,6} and Yasuhiro Hatsugai^{3,4}

¹*Computational Materials Science Research Team,
RIKEN Center for Computational Science (R-CCS), Kobe, Hyogo 650-0047, Japan*

²*Quantum Computational Science Research Team,
RIKEN Center for Quantum Computing (RQC), Wako, Saitama 351-0198, Japan*

³*Graduate School of Pure and Applied Sciences, University of Tsukuba, Tsukuba, Ibaraki 305-8571, Japan*

⁴*Department of Physics, University of Tsukuba, Tsukuba, Ibaraki 305-8571, Japan*

⁵*Computational Condensed Matter Physics Laboratory, RIKEN, Wako, Saitama 351-0198, Japan*

⁶*Computational Quantum Matter Research Team,
RIKEN Center for Emergent Matter Science (CEMS), Wako, Saitama 351-0198, Japan*

(Dated: October 26, 2021)

We provide the first unbiased evidence for a higher-order topological Mott insulator in three dimensions by numerically exact quantum Monte Carlo simulations. This insulating phase is adiabatically connected to a third-order topological insulator in the noninteracting limit, which features gapless modes around the corners of the pyrochlore lattice and is characterized by a \mathbb{Z}_4 spin-Berry phase. The difference between the correlated and non-correlated topological phases is that in the former phase the gapless corner modes emerge only in spin excitations being Mott-like. We also show that the topological phase transition from the third-order topological Mott insulator to the usual Mott insulator occurs when the bulk spin gap solely closes.

INTRODUCTION

Nontrivial topological properties and many-body effects are the two major subjects in modern condensed matter physics. In a system involving these two subjects, obtaining knowledge of a wave function, often required for characterizing topological properties, is difficult and demanding because of the many-body nature. In such a situation, the adiabatic-connection approach and the notion of bulk-edge correspondence can still provide smoking-gun evidence for an interacting topological phase.

The topological Mott insulator (TMI) is a novel state of matter in which nontrivial topological properties and correlation effects coexist [1–3]. Such a state was first proposed by Pesin and Balents as one of possible ground states for Ir-based pyrochlore oxides [4]. Among various interesting issues originated in their proposal, gapless surface spin-only excitations in the TMI are intriguing, since it is in sharp contrast to the case of the usual topological insulators where gapless edge excitations appear in the single-particle spectrum [5–7]. Namely, in the TMI, the bulk-edge (boundary) correspondence [8, 9], one of the most distinguished and ubiquitous properties of the topological insulators, is generalized by the correlation effect. Soon after the proposal, intensive studies have examined the possibility of TMI in several condensed matter systems [10–20], yielding concrete evidences for one [17] and two [18–20] dimensional cases. However, the TMI in three dimensions (3D) has not yet been fully explored, partly because of lack of reliable methods to study the correlated systems in 3D such as the complicated model considered for the Ir oxides [4].

On the one hand, recently, another type of unconven-

tional topological insulators, a higher-order topological insulator (HOTI), has been attracting increasing interest [21, 22]. The n th-order topological insulator in d -dimensions features gapless excitations around its $(d-n)$ -dimensional boundaries. Thus, also in HOTI, the bulk-edge correspondence is generalized. The studies of the HOTI have not always been material-oriented [23–28], but also have covered a wide range of models [21, 22, 29–49] and experimental setups [50–57]. Among them, three of the present authors proposed a tailored model to investigate the correlation effects on the HOTI in $d = 2$ and found a correlated topological state dubbed as a higher-order topological Mott insulator (HOTMI), in which gapless corner modes emerge only in spin excitations [45].

In this study, we present unbiased numerical evidence for a HOTMI in 3D by constructing a repulsive Hubbard model with spin-dependent hoppings on the pyrochlore lattice. Our results support the TMI in 3D in the sense that, both in the TMI and the HOTMI, the nontrivial bulk topological property manifests itself in the edge states only through the spin channel. As in the case of the kagome lattice [45], the repulsive Hubbard model with spin-dependent hoppings on the pyrochlore lattice can be mapped into the attractive Hubbard model by the particle-hole transformation, and hence we can utilize a quantum Monte Carlo (QMC) method for the correlated model in 3D without facing the negative-sign problem. We show that the on-site interaction (U) added to the HOTI closes neither the charge nor spin gap in the bulk, which suggests that the higher-order topology characterized by a \mathbb{Z}_4 spin-Berry phase [58] in the HOTI is adiabatically preserved in the $U > 0$ phase. As for the properties around the boundaries, the characteristic gapless corner modes are found only in the spin sector. These results indicate that the $U > 0$ phase, next to the HOTI,

is the third-order topological Mott insulator in 3D. We also show that the gapless corner modes disappear when the bulk spin gap vanishes at a phase boundary between the HOTMI and the Mott insulator (MI).

RESULTS

Model

We study the spinful interacting model on the pyrochlore lattice. The Hamiltonian is described by

$$\mathcal{H} = \mathcal{H}_t^\Delta + \mathcal{H}_t^\nabla + \mathcal{H}_U - \mu N - h S_{\text{tot}}^z, \quad (1)$$

with

$$\mathcal{H}_t^\Gamma = -t_\Gamma \sum_{i,j \in \Gamma} \sum_{\alpha, \beta = \uparrow, \downarrow} \left(c_{i\alpha}^\dagger \sigma_{\alpha\beta}^z c_{j\beta} + \text{h.c.} \right) \quad (2)$$

and

$$\mathcal{H}_U = U \sum_i \left(n_{i\uparrow} - \frac{1}{2} \right) \left(n_{i\downarrow} - \frac{1}{2} \right), \quad (3)$$

where $c_{i\alpha}^\dagger$ creates an electron with spin α ($=\uparrow, \downarrow$) at site i , $\sigma_{\alpha\beta}^z$ is the z -component of Pauli matrix, and $n_{i\alpha} = c_{i\alpha}^\dagger c_{i\alpha}$ is a number operator. Since we consider the model in the grand canonical ensemble, we explicitly include the terms for a chemical potential μ and a magnetic field h , which are coupled to the total number of the electrons, $N = \sum_{i\alpha} n_{i\alpha}$, and the total magnetization, $S_{\text{tot}}^z = \sum_i (n_{i\uparrow} - n_{i\downarrow})/2$. In the kinetic part \mathcal{H}_t^Γ with $\Gamma = \Delta$ and ∇ , t_Δ and t_∇ denotes the transfer integrals for the intra and inter unit cell, respectively [see Fig. 1(a)]. Their relative ratio is parameterized by ϕ with $0 \leq \phi \leq 1/2$ as $t_\Delta = t \sin(\phi\pi)$ and $t_\nabla = t \cos(\phi\pi)$. Here, t is chosen as an energy unit, namely, $t = 1$. The Hubbard term of Eq. (3) represents the repulsive (> 0) on-site interaction.

The system preserves a certain type of particle-hole symmetry defined by a transformation of $c_{i\uparrow} \rightarrow \tilde{c}_{i\downarrow}^\dagger$ and $c_{i\downarrow} \rightarrow \tilde{c}_{i\uparrow}^\dagger$, under which the Hamiltonian is invariant for $\mu = 0$. The number of electrons with spin up, $\langle n_{i\uparrow} \rangle$, where $\langle \dots \rangle$ denotes an expectation value defined below, is related to that for spin down in the transformed Hamiltonian as $\langle n_{i\uparrow} \rangle = 1 - \langle \tilde{n}_{i\downarrow} \rangle$. Since the invariant Hamiltonian trivially yields the same expectation value, $\langle \tilde{n}_{i\downarrow} \rangle = \langle n_{i\downarrow} \rangle$, the system is half filled, i.e., $\langle n_{i\uparrow} \rangle + \langle n_{i\downarrow} \rangle = 1$, at $\mu = 0$, which is the case we consider in this study.

The unusual ingredient in our model would be $\sigma_{\alpha\beta}^z$ in Eq. (2), which simply leads to the spin-dependent transfer integrals. Such a modification of the model was proposed in the previous study [45] for the kagome lattice to induce the bulk gap in the single-particle spectrum, necessary for realizing the topological phases. In this

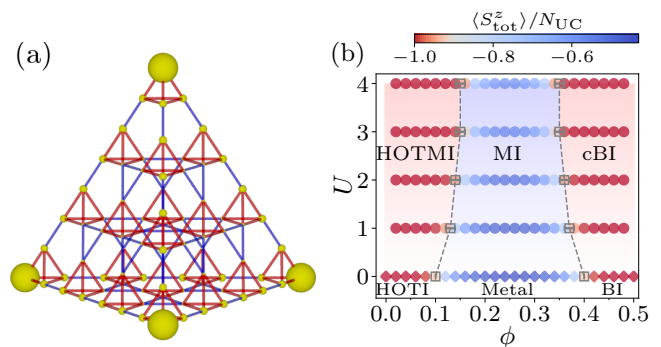


FIG. 1. (a) Pyrochlore lattice for $L = 4$ with the open boundary conditions. The small upward tetrahedron represents the unit cell. Transfer integral for the intra (inter) unit cell indicated by red (blue) is t_Δ (t_∇). Enhancement of the local moment by the on-site interaction $U = 1$, i.e., $\langle m_i^z \rangle_{U=1} - \langle m_i^z \rangle_{U=0}$, is shown by the radius of the yellow spheres for $\phi = 0.08$ and $T = 0.08$. (b) Ground-state phase diagram as function of ϕ and U . The color of the two symbols, circles for $U > 0$ and diamonds at $U = 0$, represents the value of $\langle S_{\text{tot}}^z \rangle / N_{\text{UC}}$.

study, $\sigma_{\alpha\beta}^z$ is also crucial for allowing the sign-problem-free QMC calculations.

We employ the finite-temperature auxiliary-field quantum Monte Carlo method [59–63]. An expectation value of a physical operator \mathcal{O} at a finite temperature T is calculated in the grand canonical ensemble as $\langle \mathcal{O} \rangle = \frac{1}{Z} \text{Tr}(\mathcal{O} e^{-\beta\mathcal{H}})$, where $Z = \text{Tr}(e^{-\beta\mathcal{H}})$ is the partition function, and $\beta = 1/T$ denotes an inverse temperature. To be convinced that our model is sign-problem free, let us consider a partial particle-hole transformation, $c_{i\uparrow} \rightarrow \tilde{c}_{i\uparrow}^\dagger$ and $c_{i\downarrow} \rightarrow \tilde{c}_{i\downarrow}^\dagger$, which maps the Hamiltonian into the following form (excluding a constant term):

$$\begin{aligned} \mathcal{H} \rightarrow \tilde{\mathcal{H}} = & - \sum_{\Gamma=\Delta, \nabla} \sum_{i,j \in \Gamma} \sum_{\alpha=\uparrow, \downarrow} t_\Gamma \left(\tilde{c}_{i\alpha}^\dagger \tilde{c}_{j\alpha} + \text{h.c.} \right) \\ & - U \sum_i \left(\tilde{n}_{i\uparrow} - \frac{1}{2} \right) \left(\tilde{n}_{i\downarrow} - \frac{1}{2} \right) \\ & - \mu \sum_i (\tilde{n}_{i\uparrow} - \tilde{n}_{i\downarrow}) - \frac{h}{2} \sum_i (\tilde{n}_{i\uparrow} + \tilde{n}_{i\downarrow}). \end{aligned} \quad (4)$$

This reads the attractive Hubbard model without the spin-dependency in the transfer integrals, therefore being free from the sign problem in the absence of the effective magnetic field, namely $\mu = 0$ [64]. It is also understood that $\langle S_{\text{tot}}^z \rangle$ is nonzero even for $h = 0$, because in terms of the attractive model, the zero chemical potential does not correspond to the half filling for non-bipartite lattices [65]. Owing to the absence of the negative sign problem, we can perform the QMC simulations for fairly large clusters with several hundreds of the lattice sites far beyond the scope of the exact diagonalization method. To study the bulk and boundary properties, we treat the model under periodic boundary conditions (PBC) and

open boundary conditions (OBC). The total number of the unit cells N_{UC} is L^3 for PBC and $L(L+1)(L+2)/6$ for OBC, where L denotes the number of the unit cells aligned in the linear dimension [see Fig. 1(a) for the case of OBC], and the total number of the lattice sites N_s is $4N_{\text{UC}}$.

Phase diagram

The model for $U > 0$ has three different phases; the HOTMI, the MI, and the correlated band insulator (cBI) as summarized in Fig. 1(b). Here, the cBI is the trivial band insulator with the charge and spin gaps, thus being different from the HOTMI or the MI. The two phase boundaries, referred to as ϕ_{c1}^U and ϕ_{c2}^U , are determined as points where the value of $\langle S_{\text{tot}}^z \rangle / N_{\text{UC}}$ deviates from -1 , which is the value of that in the HOTI or the band insulator (BI) at $U = 0$ [66]. This is because the HOTMI (cBI) is smoothly connected from the HOTI (BI) and is therefore labeled by the same value of $\langle S_{\text{tot}}^z \rangle$. The phase boundaries thus determined are legitimated by calculating a more direct quantity, i.e., the spin gap, from magnetization plateaus under the nonzero magnetic field h [66].

HOTI at $U = 0$

There are three phases at $U = 0$ when ϕ is varied: the HOTI, the metal, and the BI, divided by $\phi_{c1}^0 \simeq 0.1$ and $\phi_{c2}^0 \simeq 0.4$. In the limit of $\phi = 0$ or $1/2$, the system is completely decoupled into a set of isolated tetrahedrons, where the energy levels in each tetrahedron is $E = -3$ (3) and 1 (-1) for up (down) spin with the latter being threefold degenerate. Consequently, both of the HOTI and the BI have $\langle S_{\text{tot}}^z \rangle / N_{\text{UC}} = -1$, since the chemical potential is set as $\mu = 0$. The difference between the two gapped phases can be determined by the \mathbb{Z}_4 spin-Berry phase [58]: $\gamma = \pi$ for the HOTI and $\gamma = 0$ for the BI. This topological invariant is defined by an integration of the many-body Berry connection associated with local gauge twists. The S_4 symmetry of the pyrochlore lattice yields its \mathbb{Z}_4 quantization as $\gamma = 2\pi n/4$ with $n = 0, 1, 2, 3$ [66].

The distinction between the HOTI and the BI can also be made by imposing the OBC, since according to the bulk-edge correspondence [8, 9] the topological property in the bulk is reflected in the edge states. The edge states of the HOTI appear as the zero-energy states in the energy spectra, whereas such states are absent in the BI [33, 66]. The zero-energy states are fourfold degenerate for each spin, originating from the isolated sites at the four corners of the finite-size cluster of the pyrochlore lattice [see Fig. 1(a)] in the limit of $\phi = 0$. Therefore, the zero-energy states for $\phi < \phi_{c1}^0$ are mostly localized at these corners [66], representing the third-order topological insulator in 3D [33].

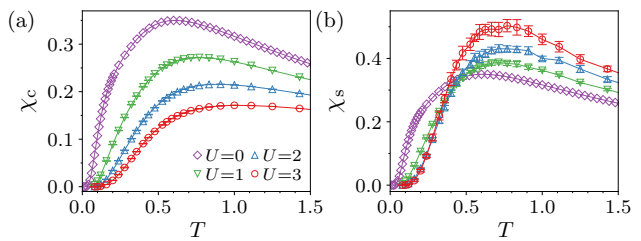


FIG. 2. Temperature dependence of (a) charge compressibility χ_c and (b) spin susceptibility χ_s at $\phi = 0.08$ for $L = 5$ under the PBC.

From HOTI to HOTMI

The HOTI changes to the HOTMI when the on-site interaction U is turned on. It is, however, difficult to distinguish these two phases by the bulk properties because they both have the charge and spin gaps. In Fig. 2, we show temperature dependence of the charge compressibility χ_c and the spin susceptibility χ_s , defined respectively as

$$\chi_c = \frac{1}{N_s} \frac{\partial \langle N \rangle}{\partial \mu} \quad (5)$$

and

$$\chi_s = \frac{1}{N_s} \frac{\partial \langle S_{\text{tot}}^z \rangle}{\partial h}, \quad (6)$$

at $\phi = 0.08 < \phi_{c1}^0$. Except that χ_c is more strongly suppressed by U , there is no obvious qualitative difference between the HOTI and the HOTMI. On the other hand, if we consider the system under the OBC, the difference can be noticeable as shown in Fig. 3. At $U = 0$, both χ_c and χ_s show a diverging behavior at low T , which is due to the gapless modes in the HOTI. For $U > 0$, the gapless charge excitations vanish as shown in Fig. 3(a), whereas the gapless spin excitations remain as evident in the diverging behavior of χ_s for $U > 0$ [see Fig. 3(b)]. The feature that the boundary states possess only the charge gap seems common in the TMI [1, 2].

The gapless modes observed from χ_c and χ_s for the system under the OBC are elucidated by “site-resolved” charge compressibility and spin susceptibility, defined respectively as

$$\kappa_c(i) = \frac{\partial \langle n_i \rangle}{\partial \mu} \quad (7)$$

and

$$\kappa_s(i) = \frac{\partial \langle m_i \rangle}{\partial h} \quad (8)$$

with $m_i = (n_{i\uparrow} - n_{i\downarrow})/2$, which are similar to a momentum-resolved compressibility [67–69]. As shown in Fig. 3(c), $\kappa_c(i)$ for $U = 0$ exhibits peaks at four site occupations that are the isolated corners in the limit of $\phi = 0$.

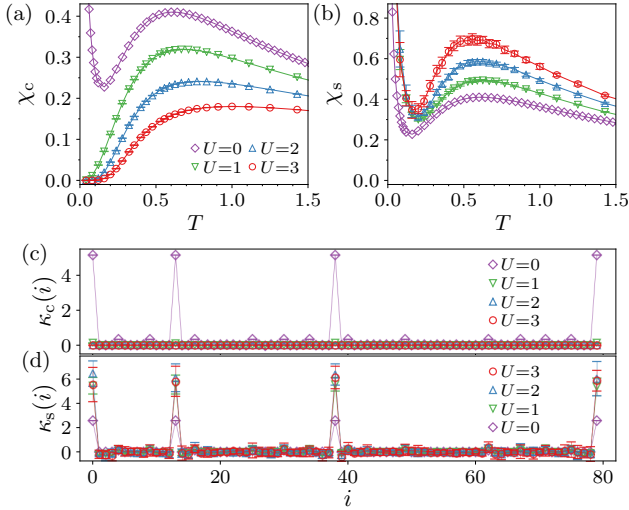


FIG. 3. Temperature dependence of (a) charge compressibility χ_c and (b) spin susceptibility χ_s at $\phi = 0.08$ for $L = 5$ under the OBC. Site-resolved (c) charge compressibility $\kappa_c(i)$ and (d) spin susceptibility $\kappa_s(i)$ for the system of $L = 4$ under the OBC at $\phi = 0.08$ and $T = 0.08$.

This is the expected behavior of the third-order topological insulator in three dimensions. Note that the peaks in $\kappa_s(i)$ of Fig. 3(d) are identical to those in $\kappa_c(i)$ (except for the constant factor) at $U = 0$ because the gapless excitations appear in the single-particle spectrum. The peaks in $\kappa_c(i)$ immediately disappear upon inclusion of U , while the peaks in $\kappa_s(i)$ remain and even develop for $U > 0$. This clearly shows that the gapless spin excitations appear around the $(d - 3)$ -dimensional boundary, namely the corners, which can also be observed from the enhancement of the local magnetic moments $\langle m_i^2 \rangle - \langle m_i^2 \rangle_0$, where $\langle \dots \rangle_0$ denotes the expectation value for $U = 0$, as shown in Fig. 1(a).

It is desired to calculate some quantity which directly characterizes the topological index such as the spin-Berry phase [58] for further identifying the $U > 0$ phase as the HOTMI. However, such calculation is not feasible because there is no established way within the framework of the auxiliary-field QMC. It is also because the system size of the pyrochlore lattice is too large to apply the exact diagonalization method, which was possible for the kagome lattice [45]. Nevertheless, it is reasonable to consider that the nontrivial topology is protected by the bulk charge and spin gaps as shown in Fig. 2.

Collapse of the HOTMI

Next, we examine how the HOTMI evolves into the MI with varying ϕ at a fixed value of $U = 3$. We confirm in Fig. 4(a) that the charge gap does not close between the HOTMI and the MI, since the temperature dependence of

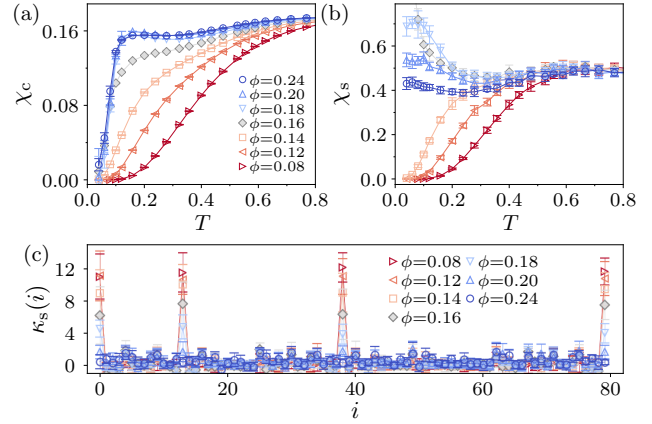


FIG. 4. Temperature dependence of (a) charge compressibility χ_c and (b) spin susceptibility χ_s for the system of $L = 5$ under the PBC at $U = 3$. (c) Site-resolved spin susceptibility $\kappa_s(i)$ for $L = 4$ under the OBC at $U = 3$ and $T = 0.08$. The critical point estimated by the value of $\langle S_{\text{tot}}^z \rangle / N_{\text{UC}}$ is $\phi_{c1}^{U=3} \simeq 0.16$.

χ_c always shows the thermally-activated behavior below and above $\phi_{c1}^U \simeq 0.16$ that is determined by $\langle S_{\text{tot}}^z \rangle / N_{\text{UC}}$. In addition, the change of χ_c with increasing ϕ is found to be nonuniform. Below ϕ_{c1}^U , χ_c gradually increases as $\phi \rightarrow \phi_{c1}^U$, indicating that the charge gap continuously decreases. At $\phi = \phi_{c1}^U$, the temperature dependence of χ_c qualitatively changes, and they fall into the almost same curve for $\phi > \phi_{c1}^U$, which suggests that the charge gap in the MI does not depend on ϕ . This abrupt change in χ_c implies that the natures of the charge gaps are different between the HOTMI and the MI. In Fig. 4(b), it is observed that the thermally-activated behavior of χ_s is completely lost for $\phi > \phi_{c1}^U$. The peak structure in $\kappa_s(i)$ also vanishes when the spin gap closes at ϕ_{c1}^U as shown in Fig. 4(c) [66]. This topological phase transition is intrinsically different from the noninteracting counterpart; while in the noninteracting systems the topological property can change when the charge and spin gaps close, here the topological phase transition occurs when the spin gap solely closes.

DISCUSSION

Finally, we comment on possible realizations of the HOTMI. The starting model of Eq. (1) involves the spin-dependent transfer integrals which seems difficult to realize in material. However, if we exploit the mapping of Eq. (4), the mapped attractive model turns out to have the hoppings which does not depend on the spin. We thus expect that the HOTMI would be realized in materials with the breathing pyrochlore lattice structure and the attractive interaction at quarter filling. Such a system may also have instability to superconductivity [70].

Then, we are also tempted to speculate that some aspects of the HOTMI on the kagome lattice [45] might be related to recently discovered kagome superconductors AV_3Sb_5 (A=K, Rb, Cs) [71–74].

We have studied the spinful Hubbard-like model on the pyrochlore lattice in three dimensions. Owing to the well-designed amendment of the model, namely the spin-dependent transfer integrals originally proposed in the previous study on the kagome lattice, the model yields the higher-order topological insulator in the noninteracting limit. The spin-dependent transfer integrals also enable us to study the model by the auxiliary-field quantum Monte Carlo method, which is numerically exact, without suffering the negative-sign problem. With including the interaction U , we have found that the gapless corner spin-only excitations persist for the system with the open boundaries, while the bulk hosts both the charge and spin gaps, which is characteristics of the topological Mott insulator. To our best knowledge, this is the first unbiased evidence for the topological Mott insulator in three dimensions. Furthermore, we have confirmed that this phase also falls within the category of the higher-order topological Mott insulator by calculating the site-resolved spin susceptibility showing the peaks at the corners. The higher-order topological Mott insulator collapses into the usual Mott insulator when the bulk spin gap solely closes.

ACKNOWLEDGMENTS

This work was supported by JSPS KAKENHI Grant Numbers JP17H06138, JP18K03475, JP18H01183, JP19J12317, JP20H04627, JP21K13850, JP21H04446, and JP21K03395. Parts of numerical simulations have been performed on the HOKUSAI supercomputer at RIKEN (Project ID: G20006) and the FUGAKU supercomputer provided by the RIKEN Center for Computational Science (R-CCS).

AUTHOR CONTRIBUTIONS

Y.O. developed the numerical codes, performed the QMC simulations, and analyzed the numerical data. All authors conceived the project and participated in the discussion of the results and in the writing of the paper.

COMPETING INTERESTS

The authors declare no competing interests.

DATA AVAILABILITY

The datasets generated and/or analyzed during the current study are available from the corresponding author on reasonable request.

-
- [1] M. Hohenadler and F. F. Assaad, *J. Phys. Condens. Matter* **25**, 143201 (2013).
 - [2] S. Rachel, *Reports Prog. Phys.* **81**, 116501 (2018).
 - [3] Note that the topological Mott insulators studied here and in Ref. 75 are different, although the same term is used. In the former case, the topological Mott insulator is found as a Mott insulator possessing gapless edge spin-only excitations, while in the latter case band topology is induced from spontaneous symmetry breaking due to interactions.
 - [4] D. A. Pesin and L. Balents, *Nat. Phys.* **6**, 376 (2009).
 - [5] M. Z. Hasan and C. L. Kane, *Rev. Mod. Phys.* **82**, 3045 (2010).
 - [6] J. E. Moore, *Nature* **464**, 194 (2010).
 - [7] X.-L. Qi and S.-C. Zhang, *Rev. Mod. Phys.* **83**, 1057 (2011).
 - [8] Y. Hatsugai, *Phys. Rev. Lett.* **71**, 3697 (1993).
 - [9] Y. Hatsugai, *Phys. Rev. B* **48**, 11851 (1993).
 - [10] Y. Yamaji and M. Imada, *Phys. Rev. B* **83**, 205122 (2011).
 - [11] M. Hohenadler, T. C. Lang, and F. F. Assaad, *Phys. Rev. Lett.* **106**, 100403 (2011).
 - [12] S.-L. Yu, X. C. Xie, and J.-X. Li, *Phys. Rev. Lett.* **107**, 010401 (2011).
 - [13] D. Zheng, G.-M. Zhang, and C. Wu, *Phys. Rev. B* **84**, 205121 (2011).
 - [14] T. Yoshida, S. Fujimoto, and N. Kawakami, *Phys. Rev. B* **85**, 125113 (2012).
 - [15] Y. Tada, R. Peters, M. Oshikawa, A. Koga, N. Kawakami, and S. Fujimoto, *Phys. Rev. B* **85**, 165138 (2012).
 - [16] T. Yoshida, R. Peters, S. Fujimoto, and N. Kawakami, *Phys. Rev. B* **87**, 085134 (2013).
 - [17] T. Yoshida, R. Peters, S. Fujimoto, and N. Kawakami, *Phys. Rev. Lett.* **112**, 196404 (2014).
 - [18] T. Yoshida and N. Kawakami, *Phys. Rev. B* **94**, 085149 (2016).
 - [19] Z. Bi, R. Zhang, Y.-Z. You, A. Young, L. Balents, C.-X. Liu, and C. Xu, *Phys. Rev. Lett.* **118**, 126801 (2017).
 - [20] R. X. Zhang, C. Xu, and C. X. Liu, *Phys. Rev. B* **235128**, 1 (2016).
 - [21] W. A. Benalcazar, B. A. Bernevig, and T. L. Hughes, *Science* **357**, 61 (2017).
 - [22] F. Schindler, A. M. Cook, M. G. Vergniory, Z. Wang, S. S. P. Parkin, B. A. Bernevig, and T. Neupert, *Sci. Adv.* **4**, eaat0346 (2018).
 - [23] F. Schindler, Z. Wang, M. G. Vergniory, A. M. Cook, A. Murani, S. Sengupta, A. Y. Kasumov, R. Deblock, S. Jeon, I. Drozdov, H. Bouchiat, S. Guéron, A. Yazdani, B. A. Bernevig, and T. Neupert, *Nat. Phys.* **14**, 918 (2018).
 - [24] C. Yue, Y. Xu, Z. Song, H. Weng, Y.-m. Lu, C. Fang, and X. Dai, *Nat. Phys.* **15**, 577 (2019).

- [25] M. J. Gray, J. Freudenstein, S. Y. F. Zhao, R. O'Connor, S. Jenkins, N. Kumar, M. Hoek, A. Kopec, S. Huh, T. Taniguchi, K. Watanabe, R. Zhong, C. Kim, G. D. Gu, and K. S. Burch, *Nano Lett.* **19**, 4890 (2019).
- [26] B. Liu, G. Zhao, Z. Liu, and Z. F. Wang, *Nano Lett.* **19**, 6492 (2019).
- [27] X.-L. Sheng, C. Chen, H. Liu, Z. Chen, Z.-M. Yu, Y. X. Zhao, and S. A. Yang, *Phys. Rev. Lett.* **123**, 256402 (2019).
- [28] C. Chen, Z. Song, J.-Z. Zhao, Z. Chen, Z.-M. Yu, X.-L. Sheng, and S. A. Yang, *Phys. Rev. Lett.* **125**, 056402 (2020).
- [29] K. Hashimoto, X. Wu, and T. Kimura, *Phys. Rev. B* **95**, 165443 (2017).
- [30] W. A. Benalcazar, B. A. Bernevig, and T. L. Hughes, *Phys. Rev. B* **96**, 245115 (2017).
- [31] Z. Song, Z. Fang, and C. Fang, *Phys. Rev. Lett.* **119**, 246402 (2017).
- [32] T. Fukui and Y. Hatsugai, *Phys. Rev. B* **98**, 035147 (2018).
- [33] M. Ezawa, *Phys. Rev. Lett.* **120**, 026801 (2018).
- [34] M. Ezawa, *Phys. Rev. B* **98**, 045125 (2018).
- [35] J. Langbehn, Y. Peng, L. Trifunovic, F. von Oppen, and P. W. Brouwer, *Phys. Rev. Lett.* **119**, 246401 (2017).
- [36] M. Ezawa, *Phys. Rev. Lett.* **121**, 116801 (2018).
- [37] M. Ezawa, *Phys. Rev. B* **97**, 155305 (2018).
- [38] E. Khalaf, *Phys. Rev. B* **97**, 205136 (2018).
- [39] T. Liu, Y.-R. Zhang, Q. Ai, Z. Gong, K. Kawabata, M. Ueda, and F. Nori, *Phys. Rev. Lett.* **122**, 076801 (2019).
- [40] D. Čalugăru, V. Juričić, and B. Roy, *Phys. Rev. B* **99**, 041301 (2019).
- [41] H. Araki, T. Mizoguchi, and Y. Hatsugai, *Phys. Rev. B* **99**, 085406 (2019).
- [42] H. Araki, T. Mizoguchi, and Y. Hatsugai, *Phys. Rev. Res.* **2**, 012009 (2020).
- [43] T. Mizoguchi, H. Araki, and Y. Hatsugai, *J. Phys. Soc. Jpn.* **88**, 104703 (2019).
- [44] Y. You, T. Devakul, F. J. Burnell, and T. Neupert, *Phys. Rev. B* **98**, 235102 (2018).
- [45] K. Kudo, T. Yoshida, and Y. Hatsugai, *Phys. Rev. Lett.* **123**, 196402 (2019).
- [46] O. Dubinkin and T. L. Hughes, *Phys. Rev. B* **99**, 235132 (2019).
- [47] J. Bibo, I. Lovas, Y. You, F. Grusdt, and F. Pollmann, *Phys. Rev. B* **102**, 041126 (2020).
- [48] C. Peng, R.-Q. He, and Z.-Y. Lu, *Phys. Rev. B* **102**, 045110 (2019).
- [49] J. Guo, J. Sun, X. Zhu, C.-A. Li, H. Guo, and S. Feng, *Quantum Monte Carlo study of higher-order topological spin phases*, arXiv:2010.05402.
- [50] S. Imhof, C. Berger, F. Bayer, J. Brehm, L. W. Molenkamp, T. Kiessling, F. Schindler, C. H. Lee, M. Greiter, T. Neupert, and R. Thomale, *Nat. Phys.* **14**, 925 (2018).
- [51] C. W. Peterson, W. A. Benalcazar, T. L. Hughes, and G. Bahl, *Nature* **555**, 346 (2018).
- [52] M. Serra-Garcia, V. Peri, R. Süsstrunk, O. R. Bilal, T. Larsen, L. G. Villanueva, and S. D. Huber, *Nature* **555**, 342 (2018).
- [53] X. Ni, M. Weiner, A. Alù, and A. B. Khanikaev, *Nat. Mater.* **18**, 113 (2019).
- [54] H. Xue, Y. Yang, F. Gao, Y. Chong, and B. Zhang, *Nat. Mater.* **18**, 108 (2019).
- [55] H. Xue, Y. Yang, G. Liu, F. Gao, Y. Chong, and B. Zhang, *Phys. Rev. Lett.* **122**, 244301 (2019).
- [56] S. N. Kempkes, M. R. Slot, J. J. van den Broeke, P. Capiod, W. A. Benalcazar, D. Vanmaekelbergh, D. Bercioux, I. Swart, C. Morais Smith, J. J. van den Broeke, P. Capiod, W. A. Benalcazar, D. Vanmaekelbergh, D. Bercioux, I. Swart, and C. M. Smith, *Nat. Mater.* **18**, 1292 (2019).
- [57] M. Weiner, X. Ni, M. Li, A. Alù, and A. B. Khanikaev, *Sci. Adv.* **6**, eaay4166 (2020).
- [58] Y. Hatsugai and I. Maruyama, *Euro. Phys. Lett.* **95**, 20003 (2011).
- [59] R. Blankenbecler, D. J. Scalapino, and R. L. Sugar, *Phys. Rev. D* **24**, 2278 (1981).
- [60] J. E. Hirsch, *Phys. Rev. B* **31**, 4403 (1985).
- [61] S. R. White, D. J. Scalapino, R. L. Sugar, E. Y. Loh, J. E. Gubernatis, and R. T. Scalettar, *Phys. Rev. B* **40**, 506 (1989).
- [62] R. Scalettar, R. Noack, and R. Singh, *Phys. Rev. B* **44**, 10502 (1991).
- [63] F. Assaad and H. Evertz, in *Comput. Many-Particle Phys.*, edited by F. H., S. R., and W. A. (Springer Berlin Heidelberg, Berlin, Heidelberg, 2008) pp. 277–356.
- [64] E. Y. Loh, J. E. Gubernatis, R. T. Scalettar, S. R. White, D. J. Scalapino, and R. L. Sugar, *Phys. Rev. B* **41**, 9301 (1990).
- [65] R. R. dos Santos, *Phys. Rev. B* **48**, 3976 (1993).
- [66] See Supplemental Material for details of the \mathbb{Z}_4 spin-Berry phase, the numerical details, and additional results.
- [67] Y. Otsuka, Y. Morita, and Y. Hatsugai, *Phys. Rev. B* **66**, 073109 (2002).
- [68] Y. Otsuka and Y. Hatsugai, *Phys. B Condens. Matter* **329-333**, 580 (2003).
- [69] Y. Morita, Y. Hatsugai, and Y. Otsuka, *Phys. Rev. B* **70**, 245101 (2004).
- [70] The superconducting phase in terms of the attractive model corresponds to a ferromagnetic state in the xy plane, which should emerge somewhere in the MI region of the phase diagram.
- [71] B. R. Ortiz, L. C. Gomes, J. R. Morey, M. Winiarski, M. Bordelon, J. S. Mangum, I. W. H. Oswald, J. A. Rodriguez-Rivera, J. R. Neilson, S. D. Wilson, E. Ertekin, T. M. McQueen, and E. S. Toberer, *Phys. Rev. Mater.* **3**, 094407 (2019).
- [72] B. R. Ortiz, P. M. Sarte, E. Kenney, S. M. L. Teicher, R. Seshadri, M. J. Graf, and S. D. Wilson, *Phys. Rev. Mater.* **5**, 034801 (2021).
- [73] Y.-X. Jiang, J.-X. Yin, M. M. Denner, N. Shumiya, B. R. Ortiz, G. Xu, Z. Guguchia, J. He, M. S. Hossain, X. Liu, J. Ruff, L. Kautzsch, S. S. Zhang, G. Chang, I. Belopolski, Q. Zhang, T. A. Cochran, D. Multer, M. Litskevich, Z.-J. Cheng, X. P. Yang, Z. Wang, R. Thomale, T. Neupert, S. D. Wilson, and M. Z. Hasan, *Nat. Mater.* **20**, 1353 (2021).
- [74] Z. Liang, X. Hou, F. Zhang, W. Ma, P. Wu, Z. Zhang, F. Yu, J.-J. Ying, K. Jiang, L. Shan, Z. Wang, and X.-H. Chen, *Phys. Rev. X* **11**, 031026 (2021).
- [75] S. Raghu, X.-L. Qi, C. Honerkamp, and S.-C. Zhang, *Phys. Rev. Lett.* **100**, 156401 (2008).

Supplemental Material: Higher-Order Topological Mott Insulator on the Pyrochlore Lattice

Yuichi Otsuka,^{1,2} Tsuneya Yoshida,^{3,4} Koji Kudo,⁴ Seiji Yunoki,^{1,2,5,6} and Yasuhiro Hatsugai^{3,4}

¹Computational Materials Science Research Team, RIKEN Center for Computational Science (R-CCS), Kobe, Hyogo 650-0047, Japan

²Quantum Computational Science Research Team, RIKEN Center for Quantum Computing (RQC), Wako, Saitama 351-0198, Japan

³Graduate School of Pure and Applied Sciences, University of Tsukuba, Tsukuba, Ibaraki 305-8571, Japan

⁴Department of Physics, University of Tsukuba, Tsukuba, Ibaraki 305-8571, Japan

⁵Computational Condensed Matter Physics Laboratory, RIKEN, Wako, Saitama 351-0198, Japan

⁶Computational Quantum Matter Research Team, RIKEN Center for Emergent Matter Science (CEMS), Wako, Saitama 351-0198, Japan

S1. \mathbb{Z}_4 SPIN-BERRY PHASE

In this appendix, we describe the definition of the spin-Berry phase γ and discuss its \mathbb{Z}_4 quantization [S1, S2]. The spin-Berry phase is given by an integration over the angles of local gauge twist defined below. Let us consider the bulk system on the pyrochlore lattice. Picking up a specific downward tetrahedron, we define a unitary operator as

$$U_-(\vec{\theta}) = \exp \left\{ i \sum_{j=1}^4 n_j^- \phi_j \right\}, \quad (\text{S1})$$

where $j = 1, \dots, 4$ is the site index of the tetrahedron, $n_j^- = n_{j\uparrow} - n_{j\downarrow}$, $\phi_j = \sum_{k=1}^j \theta_k$, and $\vec{\theta} = (\theta_1, \theta_2, \theta_3, \theta_4)$ is a four-dimensional parameter defined on a torus T^4 . Setting $\mu = h = 0$ in Eq. (1), we then rewrite the Hamiltonian as

$$\mathcal{H}(\vec{\theta}) = \mathcal{H}_t^\Delta + U_-(\vec{\theta}) \mathcal{H}_t^\nabla U_-^\dagger(\vec{\theta}) + \mathcal{H}_U. \quad (\text{S2})$$

This modification brings the Peierls phase in the hopping term within the chosen downward tetrahedron as shown in Fig. S1(a). Let us define the spin-Berry connection as

$$\vec{A}(\vec{\theta}) = \langle G(\vec{\theta}) | \vec{\nabla}_{\vec{\theta}} | G(\vec{\theta}) \rangle, \quad (\text{S3})$$

where $\vec{\nabla}_{\vec{\theta}} = (\partial/\partial\theta_1, \dots, \partial/\partial\theta_4)$ and $|G(\vec{\theta})\rangle$ is the ground state of $\mathcal{H}(\vec{\theta})$. The spin-Berry phase is defined as

$$\gamma_i = \frac{1}{i} \int_{L_i} d\vec{\theta} \cdot \vec{A}(\vec{\theta}). \quad (\text{S4})$$

The integration path L_i is given as follows. Defining five points in the parameter space as

$$\begin{aligned} E_1 &= (2\pi, 0, 0, 0), \\ E_2 &= (0, 2\pi, 0, 0), \\ E_3 &= (0, 0, 2\pi, 0), \\ E_4 &= (0, 0, 0, 2\pi), \\ G &= \frac{1}{4}(2\pi, 2\pi, 2\pi, 2\pi), \end{aligned}$$

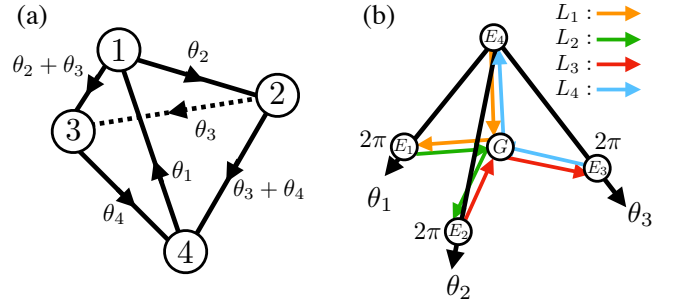


FIG. S1. (a) Peierls phase in a downward tetrahedron of the pyrochlore lattice. (b) Integration paths L_1, \dots, L_4 . G represents the center of gravity.

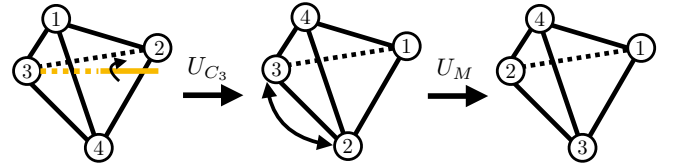


FIG. S2. Unitary operators U_{C_3} and U_M .

we introduce paths from E_i to G as shown in Fig. S1(b) by setting $\phi_4 = 2\pi$, i.e., $\theta_4 = 2\pi - \theta_1 - \theta_2 - \theta_3$. They are expressed as [S3]

$$\begin{aligned} \vec{f}_1(t) &= \frac{2\pi}{4} (4 - 3t, t, t, t), \\ \vec{f}_2(t) &= \frac{2\pi}{4} (t, 4 - 3t, t, t), \\ \vec{f}_3(t) &= \frac{2\pi}{4} (t, t, 4 - 3t, t), \\ \vec{f}_4(t) &= \frac{2\pi}{4} (t, t, t, 4 - 3t), \end{aligned}$$

where $0 \leq t \leq 1$. Along these lines, the integral path is defined as $L_i : E_{i-1} \rightarrow G \rightarrow E_i$, where $E_0 \equiv E_4$.

Due to the equivalence of the paths L_1, \dots, L_4 , the spin-Berry phase is quantized into \mathbb{Z}_4 . Let us now derive

in detail. Tetrahedron is invariant for any exchange of the vertexes by the symmetric group S_4 [S1]. This implies that the original Hamiltonian $\mathcal{H}(\vec{\theta} = \vec{0})$ have C_3 symmetry and mirror symmetry with respect to the chosen downward tetrahedron, see Fig. S2. With finite $\vec{\theta}$, the symmetry is broken but instead we have

$$(U_M U_{C_3})H(\vec{\theta})(U_M U_{C_3})^{-1} = H(g\vec{\theta}), \quad (\text{S5})$$

where g is the 4×4 unitary matrix satisfying $g\vec{\theta} = (\theta_4, \theta_1, \theta_2, \theta_3)$. Clearly, we have

$$g\vec{f}_i(t) = \vec{f}_{i+1}(t), \quad (\text{S6})$$

where $i = 1, \dots, 4$ and $\vec{f}_5 \equiv \vec{f}_1$. This implies $\gamma_1 \equiv \gamma_2 \equiv \gamma_3 \equiv \gamma_4 \equiv \gamma \pmod{2\pi}$ as follows:

$$\begin{aligned} \gamma_i &= \sum_j \frac{1}{i} \int_{L_i} d\theta_j \langle G(\vec{\theta}) | \frac{\partial}{\partial \theta_j} | G(\vec{\theta}) \rangle \\ &= \sum_j \frac{1}{i} \int_{L_{i-1}} d \left(\sum_k g_{jk} \theta_k \right) \times \\ &\quad \langle G(g\vec{\theta}^j) | \sum_l (g^{-1})_{lj} \frac{\partial}{\partial \theta_l'} | G(g\vec{\theta}^j) \rangle \\ &= \sum_{jkl} g_{jk} (g^{-1})_{lj} \frac{1}{i} \int_{L_{i-1}} d\theta_k' \langle G(g\vec{\theta}^j) | \frac{\partial}{\partial \theta_l'} | G(g\vec{\theta}^j) \rangle \\ &= \sum_l \frac{1}{i} \int_{L_{i-1}} d\theta_l' \langle G(g\vec{\theta}^j) | \frac{\partial}{\partial \theta_l'} | G(g\vec{\theta}^j) \rangle \\ &= \sum_l \frac{1}{i} \int_{L_{i-1}} d\theta_l' \langle G(\vec{\theta}^j) | \frac{\partial}{\partial \theta_l'} | G(\vec{\theta}^j) \rangle \\ &= \gamma_{i-1}, \end{aligned}$$

where $\vec{\theta} = g\vec{\theta}^j$, and we use $\partial/(\partial\theta_l')|G(g\vec{\theta}^j)\rangle = (U_M U_{C_3})^{-1} \partial/(\partial\theta_l')|G(\vec{\theta}^j)\rangle$. Since the sum of the loop L_1, \dots, L_4 is equal to zero, implying

$$\sum_i \gamma_i \equiv 0 \pmod{2\pi}, \quad (\text{S7})$$

we have

$$\gamma \equiv \frac{n}{4} 2\pi \pmod{2\pi}, \quad (\text{S8})$$

where $n = 0, 1, 2, 3$.

Since the quantized value does not change unless the energy gap closes, γ is an adiabatic invariant for gapped topological phases. For $U = 0$, we have $\gamma = \pi$ for the HOTI while $\gamma = 0$ for the band insulator. Let us now demonstrate it based on the decoupled limit. The HOTI phase includes the decoupled system with $t_\Delta = 0$, whose Hamiltonian is given by $\mathcal{H}(\vec{\theta}) = U_-(\vec{\theta})\mathcal{H}_t^\nabla U_-^\dagger(\vec{\theta})$. The

spin-Berry connection $\vec{A} = (A_1, \dots, A_4)$ is calculated as

$$\begin{aligned} A_j(\vec{\theta}) &= \langle G(\vec{\theta}) | \frac{\partial}{\partial \theta_j} | G(\vec{\theta}) \rangle = \langle G_0 | U_-^\dagger(\vec{\theta}) \frac{\partial}{\partial \theta_j} U_-(\vec{\theta}) | G_0 \rangle \\ &= \langle G_0 | \left(i \sum_{k=j}^4 n_k^- \right) | G_0 \rangle, \end{aligned}$$

where $|G_0\rangle = |G(\vec{\theta} = \vec{0})\rangle$. Because of symmetry, we have $\langle G_0 | n_1^- | G_0 \rangle = \dots = \langle G_0 | n_4^- | G_0 \rangle \equiv s$ and

$$A_j(\vec{\theta}) = i(5-j)s. \quad (\text{S9})$$

Consequently, the \mathbb{Z}_4 spin-Berry phase is given by

$$\begin{aligned} \gamma_1 &= \frac{1}{i} \int_{L_1} d\vec{\theta} \cdot \vec{A}(\vec{\theta}) \\ &= \frac{1}{i} \int_0^{2\pi} d\theta_1 A_1(\vec{\theta}) + \frac{1}{i} \int_{2\pi}^0 d\theta_4 A_4(\vec{\theta}) \\ &= \frac{1}{i} \int_0^{2\pi} d\theta_1 (i4s) + \frac{1}{i} \int_{2\pi}^0 d\theta_4 (is) \\ &= 6\pi s. \end{aligned} \quad (\text{S10})$$

As mentioned in the main text, we have $s = -1/2$ in the half-filling, which implies $\gamma = \pi \pmod{2\pi}$. The other limit, i.e., $t_\nabla = 0$ is included in the band insulating phase. Its Hamiltonian is given by $H(\vec{\theta}) = H^\Delta$. Because of the independence of $\vec{\theta}$, we have $\gamma = 0 \pmod{2\pi}$.

S2. COMPUTATIONAL DETAILS OF QMC SIMULATIONS

In the scheme of the auxiliary field QMC, the Suzuki-Trotter decomposition [S4, S5] is first applied to $e^{-\beta\mathcal{H}}$ as $e^{-\beta\mathcal{H}} \simeq \prod e^{-\Delta\tau\mathcal{H}_t/2} e^{-\Delta\tau\mathcal{H}_U} e^{-\Delta\tau\mathcal{H}_t/2}$, where \mathcal{H}_t stands for the noninteracting parts in \mathcal{H} , and $\Delta\tau = \beta/M$ is a Trotter slice with M being integer. The discrete Hubbard-Stratonovich transformation [S6] is then applied to each term of $e^{-\Delta\tau U n_i \uparrow n_i \downarrow}$, introducing an auxiliary Ising-type variable at each spatial site in each imaginary time slice. The summation over the auxiliary fields involving the MN_s Ising variables is performed by Monte Carlo (MC) sampling.

We set the Trotter slice as $\Delta\tau = 0.1$, for which the Trotter errors of order $O(\Delta\tau^2)$ are sufficiently small compared with statistical errors of the MC sampling. As for the Hubbard-Stratonovich transformation, we employ one which couples to the spin degree of freedom. Typically, we perform 4×10^3 MC sweeps for equilibration, followed by 8×10^4 MC sweeps for measurement, which are divided into 20 bins to estimate the statistical error by the standard deviation. Each MC sweep consists of MN_s local updates and N_s global moves [S7]. The simulations are carried out on the finite size clusters with L up to 5 (8) corresponding to $N_s = 500$ (480) under the PBC (OBC).

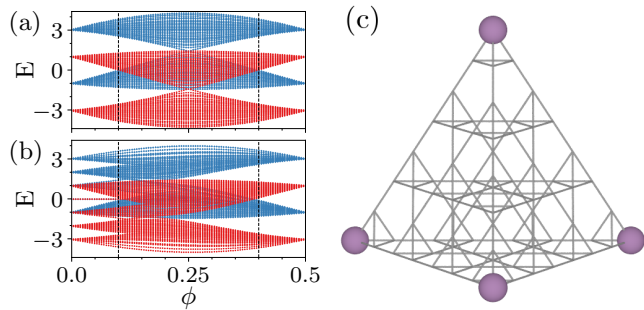


FIG. S3. Energy spectra as function of ϕ at $U = 0$ for (a) $L = 10$ under the PBC and (b) $L = 8$ under the OBC. Red (blue) symbols represent the energy levels for up (down) spin. Vertical dashed lines indicate $\phi_{c1}^0 \simeq 0.1$ and $\phi_{c2}^0 \simeq 0.4$. (c) The averaged probability densities of the degenerated zero-energy states for $L = 4$ under the OBC are shown by the radius of the purple spheres for $\phi = 0.04$.

S3. ENERGY SPECTRA AT $U = 0$

The energy spectra as function of ϕ in the noninteracting limit are shown in Fig. S3. For the system under the PBC, the single-particle gap opens for the HOTI of $\phi < \phi_{c1}^0 \simeq 0.1$ and the BI of $\phi > \phi_{c2}^0 \simeq 0.4$. For the system under the OBC, the eightfold degenerate zero-energy states appear only in the HOTI. The averaged probability densities of these degenerated states are shown in Fig. S3(c) for $\phi = 0.04$.

S4. DETERMINATION OF PHASE BOUNDARIES

As shown in Fig. S4, we find $\phi_{c1}^U = 0.15(1)$ and $0.13(1)$ for $U = 3$ and 1 . Above ϕ_{c1}^U , the strong finite-size effect is observed at low T [see Figs. S4(c) and S4(f)], implying the absence of the bulk spin gap.

S5. COLLAPSE OF SPIN GAP

We confirm that the spin gap indeed vanishes at $\phi = \phi_{c1}^U$ from magnetization plateaus under the magnetic field h as shown in Fig. S5. It is noted that the simulations for $h \neq 0$ are possible without encountering the negative sign problem, since the model can be mapped onto the attractive model. The critical magnetic field, h_c , is determined, in the similar way to ϕ_{c1}^U , as the point above which $\langle S_{\text{tot}}^z \rangle / N_{\text{UC}}$ deviates from -1 . Since the spin gap is proportional to h_c , the ϕ -dependence of h_c in Fig. S5(c) represents how the spin gap decreases. Thus, the critical point ϕ_{c1}^U is estimated as the point of ϕ for which h_c is zero. The result in Fig. S5(c) shows that ϕ_{c1}^U estimated in this way turn out to agree well with those obtained from the T -dependence of $\langle S_{\text{tot}}^z \rangle / N_{\text{UC}}$ in Fig. S4 within

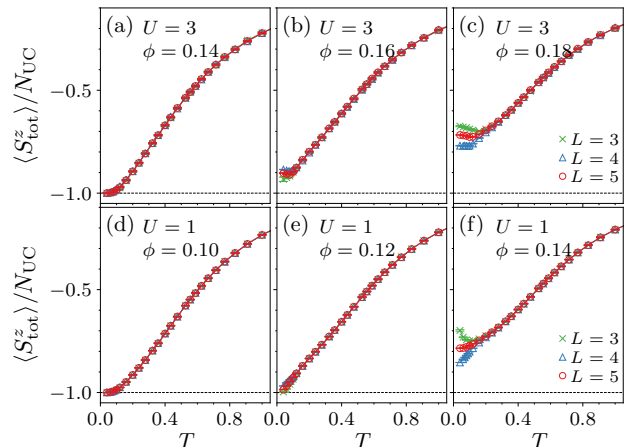


FIG. S4. Temperature dependence of $\langle S_{\text{tot}}^z \rangle / N_{\text{UC}}$ for various values of ϕ under the PBC. Upper [(a)-(c)] and lower [(d)-(f)] panels show the results of $U = 3$ and $U = 1$, respectively. The horizontal dashed lines indicate $\langle S_{\text{tot}}^z \rangle / N_{\text{UC}} = -1$, which is the value of the ground-state in the HOTMI phase.

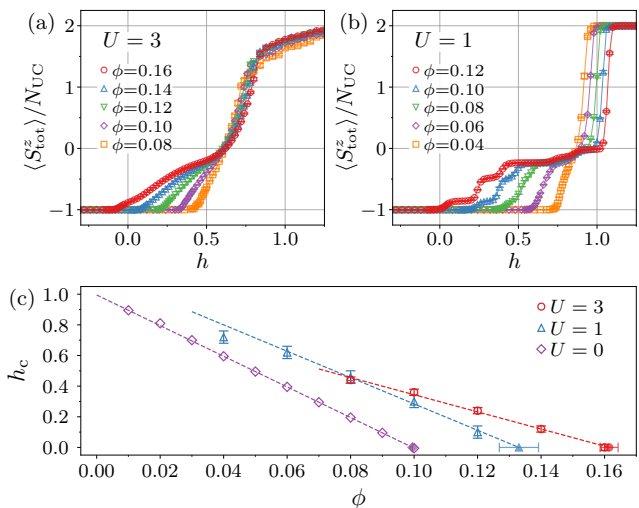


FIG. S5. $\langle S_{\text{tot}}^z \rangle / N_{\text{UC}}$ as a function of the magnetic field h for (a) $U = 3$ and (b) $U = 1$, and $L = 4$ under the PBC at $T = 0.025$, from which the critical magnetic fields h_c are determined. (c) ϕ -dependence of h_c for $U = 3$ and 1 . For comparison, corresponding exact values for $U = 0$ are also shown. The dashed lines are linear fits to the data points. The filled symbols at $h_c = 0$ indicate ϕ_{c1}^U estimated from the fittings.

the error bars.

-
- [S1] Y. Hatsugai and I. Maruyama, *Euro. Phys. Lett* **95**, 200003 (2011).
 - [S2] K. Kudo, Ph. D. thesis (University of Tsukuba, 2021).
 - [S3] H. Araki, private communication.

- [S4] M. Suzuki, *Commun. Math. Phys.* **51**, 183 (1976).
[S5] H. F. Trotter, *Proc. Am. Math. Soc.* **10**, 545 (1959).
[S6] J. E. Hirsch, *Phys. Rev. B* **28**, 4059 (1983).

- [S7] R. Scalettar, R. Noack, and R. Singh, *Phys. Rev. B* **44**, 10502 (1991).